Applied Physics Letters

Elastic stiffening induces one-dimensional phonons in thin Ta_2Se_3 nanowires

Cite as: Appl. Phys. Lett. **120**, 062201 (2022); https://doi.org/10.1063/5.0083980
Submitted: 31 December 2021 • Accepted: 30 January 2022 • Published Online: 10 February 2022

Zhiliang Pan, Seng Huat Lee, Ke Wang, et al.

Applied Physics Letters ARTICLE scitation.org/journal/apl

Elastic stiffening induces one-dimensional phonons in thin Ta_2Se_3 nanowires

Cite as: Appl. Phys. Lett. **120**, 062201 (2022); doi: 10.1063/5.0083980
Submitted: 31 December 2021 · Accepted: 30 January 2022 ·
Published Online: 10 February 2022

View Online Export Citation CrossMark

Zhiliang Pan,[1] Seng Huat Lee,[2] Ke Wang,[3] Zhiqiang Mao,[2] and Deyu Li[1,a)]

AFFILIATIONS

[1]Department of Mechanical Engineering, Vanderbilt University, Nashville, Tennessee 37235, USA
[2]Department of Physics, Pennsylvania State University, University Park, Pennsylvania 16802, USA
[3]Materials Research Institute, Pennsylvania State University, University Park, Pennsylvania 16802, USA

Note: This paper is part of the APL Special Collection on One-Dimensional van der Waals Materials.
[a)]**Author to whom correspondence should be addressed:** deyu.li@vanderbilt.edu

ABSTRACT

Compared to extensive studies of thermal transport in two-dimensional materials, very limited attention has been paid to the corresponding phenomenon in quasi-one-dimensional van der Waals crystals. Here, we show that Ta_2Se_3 can be easily exfoliated into thin nanowires, indicating strong anisotropy in the bonding strength within the basal plane. Systematic thermal property measurements disclose signatures of one-dimensional phonons as the nanowire hydraulic diameter reduces below 19.2 nm with linearly escalating thermal conductivity as temperature increases and size dependence inconsistent with the classical size effect. We further show that these unusual transport properties are induced by elastic stiffening occurring for wires of <30 nm diameter.

Confined transport of energy carriers in low-dimensional materials could induce unusual phenomena that are not consistent with traditional wisdom, leading to properties promising for various applications.[1–3] In the past two decades, extensive efforts have been carried out to explore and understand thermal transport through a plethora of two-dimensional (2D) materials,[4–12] while experimental studies of one-dimensional (1D) transport have been largely limited to earlier studies of thermal transport through single-walled carbon or boron nitride nanotubes.[13–15] Only very recently, attempts to probe thermal transport in quasi-1D van der Waals (vdW) crystal nanowires have been made, which reveal interesting observations.[16–18]

For example, Zhang *et al.* first disclosed pronounced diameter and length dependence for the thermal conductivity of vdW crystal $Ta_2Pd_3Se_8$ nanowires.[16] It was shown that the thermal conductivity increases with the wire hydraulic diameter up to 110 nm and displays a length dependence beyond 13 μm at room temperature. Taking advantage of the unique charge density wave behavior in quasi-1D $NbSe_3$ nanowires, Yang *et al.* illustrated distinct signatures of electron–phonon scattering in the lattice thermal conductivity.[17] Probably, the most exciting discovery is the recent demonstration of superdiffusive phonon transport in ultrathin ($\sim$10 nm) $NbSe_3$ nanowires with the thermal conductivity (κ) escalating with the wire length (L) following a 1/3 power law of $\kappa \sim L^{1/3}$ from $\sim$6 to $>$42.5 μm, which provides solid experimental evidence to the long-standing theoretical prediction of divergent thermal conductivity of 1D lattices.[18]

Given that quasi-1D vdW crystals represent a large class of materials, it would be interesting to explore thermal transport in other vdW nanowires to further understand phonon properties in different quasi-1D materials and the size effect on thermal transport properties. Here, we show that elastic stiffening in thin Ta_2Se_3 nanowires promotes the contribution of 1D phonons at elevated temperatures with the diameter dependence of thermal conductivity violating the trend predicted based on the classical size effect.

Very little information is available for Ta_2Se_3 in the literature. A recent report using first-principles calculations predicted monolayer Ta_2Se_3 as 2D semimetals with two Dirac points close to the Fermi level.[19] However, we found that it is very easy to obtain Ta_2Se_3 nanowires from bulk single crystal needles through mechanical exfoliation using two pieces of polydimethylsiloxane (PDMS), which suggests strong anisotropy of the bonding strength along two different crystalline directions within the basal plane. The single crystalline nature of the resulting nanowires is verified by the selected area electron diffraction (SAED) pattern, and the wire axial direction can be identified from the high-resolution transmission electron microscopy (HRTEM) micrograph, as shown in Fig. 1(a).

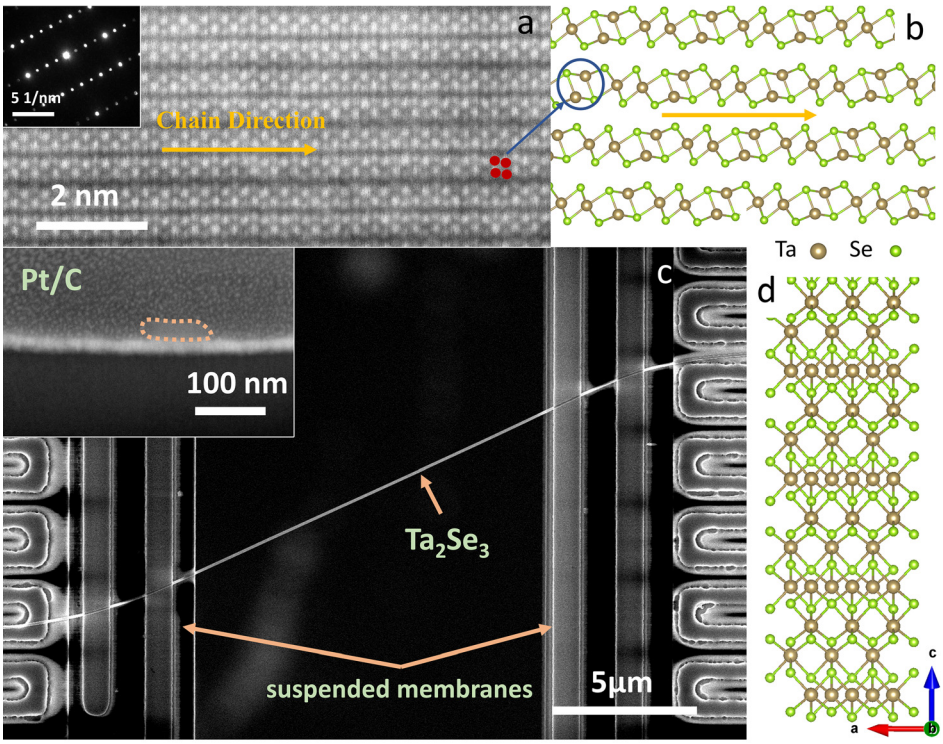

FIG. 1. (a) An HRTEM image of a Ta_2Se_3 nanowire showing the well-aligned molecular chains. Inset: SAED pattern. (b) and (d) Schematic diagram illustrating the crystalline structure of Ta_2Se_3. (c) A SEM image of the measurement device with a Ta_2Se_3 nanowire placed between the two suspended membranes (gap distance: ~12 μm). Inset: cross-sectional image of the measured nanowire.

We measured the electrical and thermal transport properties of a series of Ta_2Se_3 nanowires with different cross-sectional sizes using a well-established microthermal bridge method.[20–22] To ensure meaningful comparison of the thermal conductivity between nanowires of different sizes, the suspended length between the heat source and heat sink as shown in Fig. 1(c) for all samples is managed to be ~13 μm during the sample preparation process. Since mechanically exfoliated vdW crystal nanowires are usually of irregular shapes, we characterized each sample after thermal measurements by cutting the wire using a focused ion beam and then directly imaging the cross section via scanning electron microscopy (SEM), as shown in the inset of Fig. 1(c).[16–18] The hydraulic diameter (D_h), four times the reciprocal of the surface-area-to-volume ratio (S/V), is chosen as the characteristic size of the nanowire as it better represents the surface effects on the transport properties, as we have done for other vdW crystal nanowires.[16–18] These nanowires tend to contact the suspended membranes with a flat edge, and the relatively large contact area leads to negligible contact thermal resistance. We have confirmed this through comparing the measured thermal resistance with and without electron beam induced deposition (EBID) treatment of the wire-membrane contacts.

The electrical resistivity of Ta_2Se_3 nanowires was measured using a standard four-point method to estimate the electron contribution to the thermal conductivity. As shown in Fig. 2(a), the electrical resistivity drops by more than three orders of magnitude as the temperature increases, from 70 596.3 at 20 to 26.1 $\mu\Omega$ m at 300 K, indicating the semiconducting nature of these Ta_2Se_3 nanowires. The electronic thermal conductivity (κ_e) is estimated according to the Wiedemann–Franz law with the Lorenz number taken as the Sommerfeld value, and the lattice thermal conductivity (κ_{ph}) is extracted through subtracting κ_e from the measured total thermal conductivity (κ_{tot}). As shown in Fig. 2(b), κ_e only contributes marginally to κ_{tot}, and the maximum contribution occurs at 300 K, which is still less than 5%. As such, we neglect the electron contribution to thermal transport in the following analysis.

Figure 3(a) depicts the temperature dependence of the measured thermal conductivity for Ta_2Se_3 nanowires of different hydraulic diameters but approximately the same length of ~13 μm. For larger wires, κ first increases to a peak value at ~60 K as a result of the rapid escalation in heat capacity and then decreases with temperature due to rapidly enhanced Umklapp scattering.[23,24] The overall curve becomes flatter as the sample size reduces even though the trend remains the same for wires of >19.2 nm hydraulic diameter, originating from the stronger boundary scattering for thinner wires. However, the decreasing trend for the 19.2 nm diameter wire disappears, and more interestingly, for the two smallest samples of 18 and 16 nm diameter, the thermal conductivity starts to escalate with temperature in the temperature range of 60–300 K. The above temperature dependence can be even more clearly seen from the normalized thermal conductivity with respect to the values at 300 K for each nanowire, as shown in Fig. 3(b). While the suppression of strong temperature dependence of κ for thinner wires is common for nanowires of different materials, once the nanowire size becomes smaller than the phonon mean free path,[16,17,25] the transition to the escalating trend is unusual for nanowires made of crystalline materials. The linearly increasing profile with temperature for the thinnest wire measured (16 nm diameter) resembles that of ultra-thin $NbSe_3$ nanowires in the regime where 1D phonons dominate the thermal transport.[18]

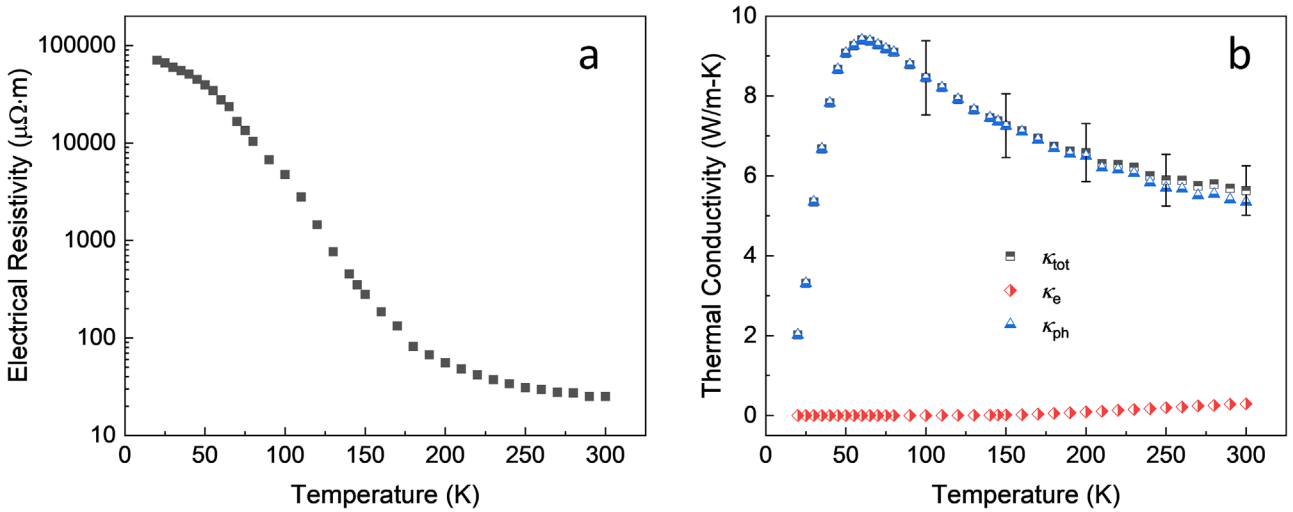

FIG. 2. (a) Electrical resistivity of a 32.7 nm diameter Ta_2Se_3 nanowire. The resistivity decreases rapidly with temperature, suggesting a semiconducting behavior. (b) Measured total thermal conductivity with contributions from phonons and electrons. Electrons contribute only a negligible portion (<5%).

To further examine the size dependence, we plot the thermal conductivity vs the wire hydraulic diameter at two different temperatures of 50 and 300 K, as shown in Fig. 4. It can be seen that at 50 K, the thermal conductivity increases monotonically with the diameter for all measured wires, which is consistent with the expectation based on the classical size effect, i.e., stronger phonon-boundary scattering from the wire surface leads to lower thermal conductivity for thinner wires. However, at 300 K, the thermal conductivity reduces as the wire hydraulic diameter drops from 50.6 to 19.2 nm, and then it starts to increase as the wire size further scales down, which is exactly opposite to the classical size effect. This deviation suggests that a certain mechanism rendering an enhanced thermal conductivity for thinner wires offsets the phonon-boundary scattering effect.

According to the kinetic theory, $\kappa_{ph} = \frac{1}{3}Cvl$, where C, v, and l are the phonon heat capacity per unit volume, group velocity, and mean free path, respectively. For the same nanowire, v usually does not change with temperature and l actually intends to decrease with temperature due to enhanced Umklapp scattering. As such, most likely the linearly escalating thermal conductivity with temperature comes from the enhanced C as temperature increases, which is consistent with the recent observation for thin $NbSe_3$ nanowires, in which 1D phonons dominate thermal transport at elevated temperatures.

It has been suggested that for $NbSe_3$ nanowires, elastic stiffening, i.e., enhanced Young's modulus (E), is responsible for the observed temperature and size dependence.[18] Higher E corresponds to an enhanced Debye temperature (θ_D), which allows for more phonon

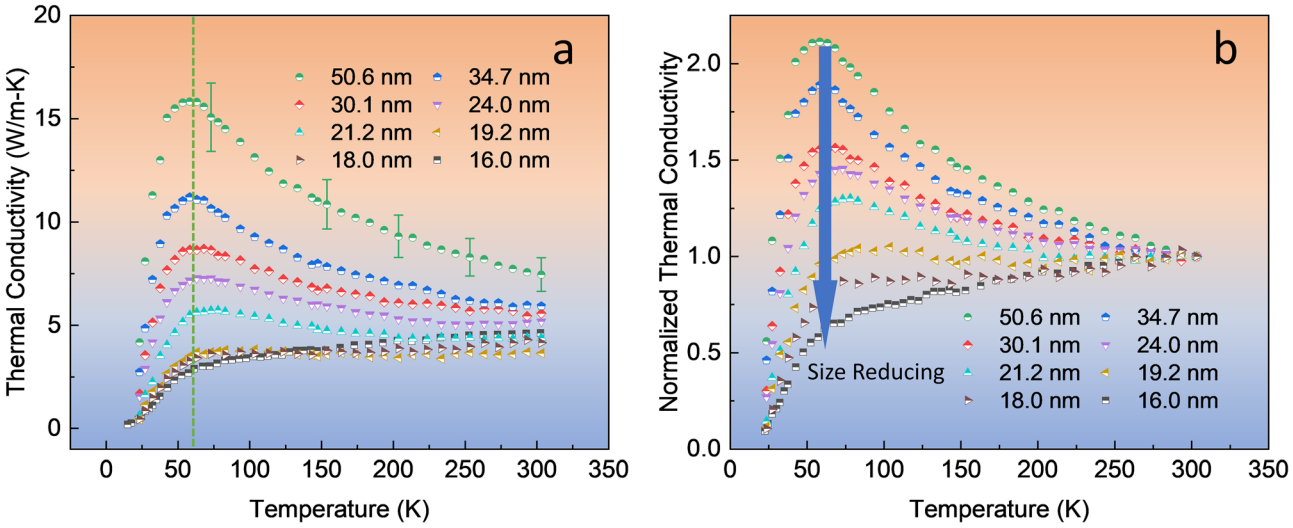

FIG. 3. (a) Thermal conductivity of different diameter Ta_2Se_3 nanowires. (b) Normalized thermal conductivity $\kappa/\kappa_{300\ K}$. A clear transition in the temperature dependence can be observed.

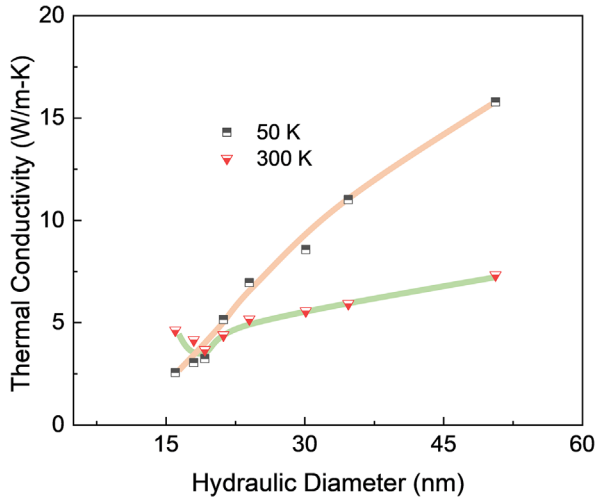

FIG. 4. Thermal conductivity of Ta_2Se_3 nanowires at 300 and 50 K. At room temperature, the thermal conductivity shows a non-monotonic size dependence while at 50 K, the thermal conductivity continuously increases with the wire size.

modes to be populated as temperature escalates, and hence an increasing heat capacity. The linearly increasing trend with temperature also suggests that the enhanced heat capacity is due to excitation of 1D phonons.

To verify that this is also the case for Ta_2Se_3 nanowires, we measured E along the sample axis direction using a three-point bending test with an atomic force microscope (AFM, Bruker Dimension Icon).[18,26–28] To do so, we placed the nanowire across a trench of ∼11 μm wide etched in a silicon substrate. Then EBID was performed to fix the two contacts between the nanowire and the trench edges, as shown in the inset of Fig. 5(a). Before each bending test, the mechanical properties of the AFM tip including the spring constant and deflection sensitivity were calibrated. To perform the bending test, the AFM tip was positioned to the middle point of the suspended wire and pushed the sample to obtain the force–deflection curve, as shown in Fig. 5(a). Young's modulus of the sample can be extracted through fitting the force–deflection curve using a theoretical model of a suspended elastic string with fixed ends.[18,26–28] The resulting Young's modulus is plotted in Fig. 5(b) vs the wire hydraulic diameter. For larger wires, E remains approximately a constant value of ∼42 GPa. However, as the hydraulic diameter drops below 30 nm, the measured E starts to increase as the sample size further reduces. For a ∼19 nm sample, E approaches ∼68 GPa, about 62% larger as compared to the value of large samples.

Coupled mechanical and thermal transport studies of nanowires have been carried out only recently with acoustic softening effects observed for silicon nanotubes and nanoribbons[22,29] and elastic stiffening effects for $NbSe_3$ and silver nanowires.[18,30] In addition to escalating the heat capacity with temperature, elastic stiffening can also lead to enhanced phonon group velocity and reduced Umklapp scattering rate. This is due to the fact that the speed of sound is proportional to $E^{1/2}$, and a higher E corresponds to a larger gap between the acoustic and optical phonon branches, which can effectively suppress Umklapp scattering.[31–33] This is because at any given temperature, a higher θ_D shifts the phonon spectrum distribution to lower wave vectors, rendering it more difficult for them to satisfy the requirements for Umklapp scattering involving optical phonons above a large energy gap.[18]

The non-monotonic size dependence at 300 K can, therefore, be attributed to the effects of elastic stiffening on thermal transport in thin Ta_2Se_3 nanowires. It is important to note that elastic stiffening also occurs at lower temperatures such as 50 K; however, no transition to higher thermal conductivity for thinner wires is observed at that temperature. This contrast suggests that the trend opposite to the classical size effect is indeed due to the 1D phonons excited at higher temperatures. However, we did notice that the slope of the curve for 50 K

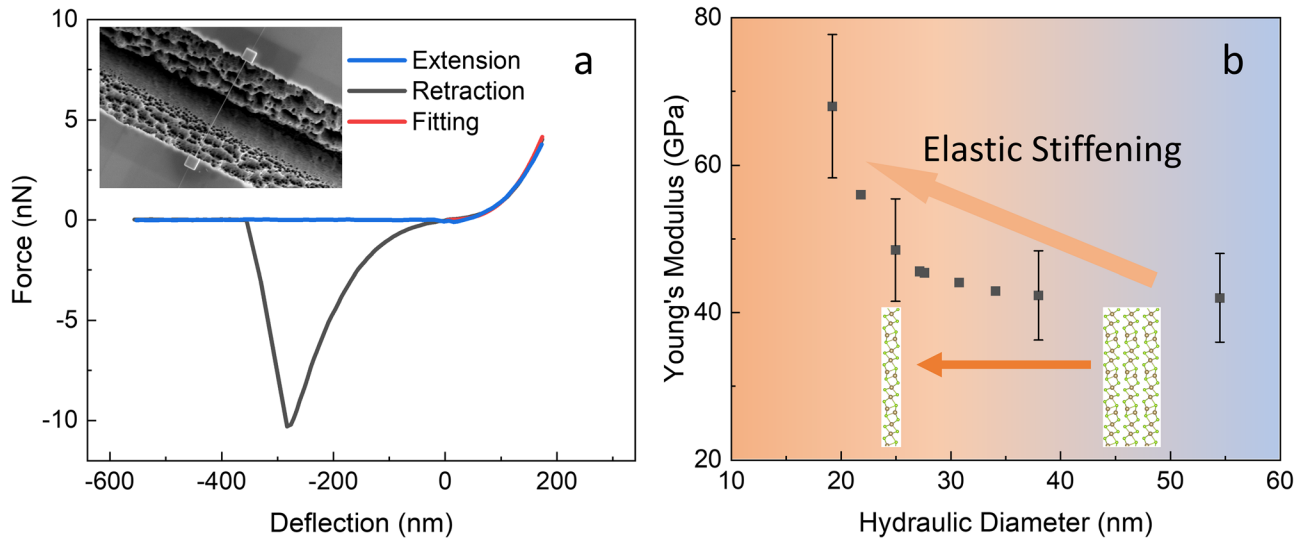

FIG. 5. (a) Force–deflection curve of a Ta_2Se_3 nanowire recorded during a three-point bending test. (b) Young's modulus data for different diameter Ta_2Se_3 nanowires. A clear increasing trend is shown as the sample size reduces.

in Fig. 4 is smaller for thinner wires, which could be attributed to that the elastic stiffening effects other than larger heat capacity partially offset the classical size effect.

We note that the thermal conductivity of the thinner Ta_2Se_3 wires is significantly lower than that of $NbSe_3$ of similar diameter.[18] For example, the room-temperature thermal conductivity of a 16 nm diameter Ta_2Se_3 nanowire is 4.63 W/m K, whereas the corresponding value for a 16 nm diameter $NbSe_3$ nanowire is 17.91 W/m K. The difference is likely due to the difference in the bonding strength. Young's modulus for a ~19 nm $NbSe_3$ nanowire is 191 GPa, 122% enhancement compared to the bulk value, whereas the enhancement is only 62% for a ~19 nm Ta_2Se_3 nanowire. A larger E enhancement can lead to a more significant thermal conductivity escalation, which can explain the difference in the observed thermal conductivity enhancement between thin Ta_2Se_3 and $NbSe_3$ nanowires.

In summary, we have experimentally shown signatures of 1D phonon transport in thin Ta_2Se_3 nanowires, which manifest as linearly increasing thermal conductivity with temperature that is opposite to the expectation from Umklapp scattering and size dependence not consistent with the classical size effect. These unusual transport properties are induced by elastic stiffening in thinner wires with an enhanced Young's modulus. The results also suggest that strong bonding anisotropy exists in Ta_2Se_3, which could behave more like quasi-1D instead of 2D crystals, especially under the effect of elastic stiffening for thinner wires. Importantly, together with the recent discovery from thin $NbSe_3$, the observation on Ta_2Se_3 suggests that elastic stiffening and 1D phonon transport could be a general feature for thin selenide-based vdW crystal nanowires. Moreover, other types of ultrathin nanowires have been experimentally demonstrated,[34–36] and it would be very interesting to explore whether signatures of 1D phonon transport could be observed in these systems.

The authors thank the financial support from the National Science Foundation (CBET Nos. 1805924 and 2114278). Support for crystal growth and characterization at Penn State was provided by the National Science Foundation through the Penn State 2D Crystal Consortium-Materials Innovation Platform (2DCC-MIP) under NSF Cooperative Agreement No. DMR-2039351.

AUTHOR DECLARATIONS

Conflict of Interest

The authors have no conflicts to disclose.

DATA AVAILABILITY

The data that support the findings of this study are available from the corresponding author upon reasonable request.

REFERENCES

[1]K. S. Novoselov, A. Mishchenko, A. Carvalho, and A. H. Castro Neto, Science **353**(6298), aac9439 (2016).
[2]H. Wang, J. Guo, J. Miao, W. Luo, Y. Gu, R. Xie, F. Wang, L. Zhang, P. Wang, and W. Hu, Small **18**, 2103963 (2021).
[3]Y. Cao, V. Fatemi, S. Fang, K. Watanabe, T. Taniguchi, E. Kaxiras, and P. Jarillo-Herrero, Nature **556**, 43–50 (2018).
[4]S. Ghosh, W. Bao, D. L. Nika, S. Subrina, E. P. Pokatilov, C. N. Lau, and A. A. Balandin, Nat. Mater. **9**, 555–558 (2010).
[5]H. Zhang, X. Chen, Y. D. Jho, and A. J. Minnich, Nano Lett. **16**, 1643–1649 (2016).
[6]Q. Fu, J. Yang, Y. Chen, D. Li, and D. Xu, Appl. Phys. Lett. **106**, 031905 (2015).
[7]A. Sood, F. Xiong, S. Chen, R. Cheaito, F. Lian, M. Asheghi, Y. Cui, D. Donadio, K. E. Goodson, and E. Pop, Nano Lett. **19**, 2434–2442 (2019).
[8]S. E. Kim, F. Mujid, A. Rai, F. Eriksson, J. Suh, P. Poddar, A. Ray, C. Park, E. Fransson, Y. Zhong, D. A. Muller, P. Erhart, D. G. Cahill, and J. Park, Nature **597**, 660–665 (2021).
[9]J. H. Seol, I. Jo, A. L. Moore, L. Lindsay, Z. H. Aitken, M. T. Pettes, X. Li, Z. Yao, R. Huang, D. Broido, N. Mingo, R. S. Ruoff, and L. Shi, Science **328**, 213–216 (2010).
[10]W. Cai, A. L. Moore, Y. Zhu, X. Li, S. Chen, L. Shi, and R. S. Ruoff, Nano Lett. **10**, 1645–1651 (2010).
[11]R. Yan, J. R. Simpson, S. Bertolazzi, J. Brivio, M. Watson, X. Wu, A. Kis, T. Luo, A. R. H. Walker, and H. G. Xing, ACS Nano **8**, 986–993 (2014).
[12]Z. Luo, J. Maassen, Y. Deng, Y. Du, R. P. Garrelts, M. S. Lundstrom, D. Y. Peide, and X. Xu, Nat. Commun. **6**, 8572 (2015).
[13]J. Hone, M. Whitney, C. Piskoti, and A. Zettl, Phys. Rev. B **59**, R2514 (1999).
[14]C. Yu, L. Shi, Z. Yao, D. Li, and A. Majumdar, Nano Lett. **5**, 1842–1846 (2005).
[15]Y. Xiao, X. H. Yan, J. X. Cao, J. W. Ding, Y. L. Mao, and J. Xiang, Phys. Rev. B **69**, 205415 (2004).
[16]Q. Zhang, C. Liu, X. Liu, J. Liu, Z. Cui, Y. Zhang, L. Yang, Y. Zhao, T. T. Xu, Y. Chen, J. Wei, Z. Mao, and D. Li, ACS Nano **12**, 2634–2642 (2018).
[17]L. Yang, Y. Tao, J. Liu, C. Liu, Q. Zhang, M. Akter, Y. Zhao, T. T. Xu, Y. Xu, Z. Mao, Y. Chen, and D. Li, Nano Lett. **19**, 415–421 (2019).
[18]L. Yang, Y. Tao, Y. Zhu, M. Akter, K. Wang, Z. Pan, Y. Zhao, Q. Zhang, Y. Xu, R. Chen, T. T. Xu, Y. Chen, Z. Mao, and D. Li, Nat. Nanotechnol. **16**, 764–765 (2021).
[19]Y. Ma, Y. Jing, and T. Heine, 2D Mater. **4**, 025111 (2017).
[20]L. Shi, D. Li, C. Yu, W. Jang, D. Kim, Z. Yao, P. Kim, and A. Majumdar, J. Heat Transfer **125**, 881–888 (2003).
[21]M. C. Wingert, Z. C. Chen, S. Kwon, J. Xiang, and R. Chen, Rev. Sci. Instrum. **83**, 024901 (2012).
[22]L. Yang, Y. Yang, Q. Zhang, Y. Zhang, Y. Jiang, Z. Guan, M. Gerboth, J. Yang, Y. Chen, D. G. Walker, T. T. Xu, and D. Li, Nanoscale **8**, 17895–17901 (2016).
[23]E. Pop, D. Mann, Q. Wang, K. Goodson, and H. Dai, Nano Lett. **6**, 96–100 (2006).
[24]L. Lindsay, D. A. Broido, and N. Mingo, Phys. Rev. B **82**, 115427 (2010).
[25]D. Li, Y. Wu, P. Kim, L. Shi, P. Yang, and A. Majumdar, Appl. Phys. Lett. **83**, 2934–2936 (2003).
[26]Q. Xiong, N. Duarte, S. Tadigadapa, and P. C. Eklund, Nano Lett. **6**, 1904–1909 (2006).
[27]Y. Calahorra, O. Shtempluck, V. Kotchetkov, and Y. E. Yaish, Nano Lett. **15**, 2945–2950 (2015).
[28]Y. E. Yaish, Y. Calahorra, O. Shtempluck, and V. Kotchetkov, J. Appl. Phys. **117**, 164311 (2015).
[29]M. C. Wingert, S. Kwon, M. Hu, D. Poulikakos, J. Xiang, and R. Chen, Nano Lett. **15**, 2605–2611 (2015).
[30]Y. Zhao, M. L. Fitzgerald, Y. Tao, Z. Pan, G. Sauti, D. Xu, Y. Xu, and D. Li, Nano Lett. **20**, 7389–7396 (2020).
[31]J. S. Kang, M. Li, H. Wu, H. Nguyen, and Y. Hu, Science **361**, 575–578 (2018).
[32]S. Li, Q. Zheng, Y. Lv, X. Liu, X. Wang, P. Y. Huang, D. G. Cahill, and B. Lv, Science **361**, 579–581 (2018).
[33]F. Tian, B. Song, X. Chen, N. K. Ravichandran, Y. Lv, K. Chen, S. Sullivan, J. Kim, Y. Zhou, T. H. Liu, M. Goni, Z. Ding, J. Sun, G. A. U. Gamage, H. Sun, H. Ziyaee, S. Huyan, L. Deng, J. Zhou, A. J. Schmidt, S. Chen, C. W. Ch, P. Huang, D. Broido, L. Shi, G. Chen, and Z. Ren, Science **361**, 582–585 (2018).
[34]X. Liu, T. Xu, X. Wu, Z. Zhang, J. Yu, H. Qiu, J. H. Hong, C. H. Jin, J. X. Li, X. R. Wang, L. T. Sun, and W. Guo, Nat. Commun. **4**, 1776 (2013).
[35]A. L. Koh, S. Wang, C. Ataca, J. C. Grossman, R. Sinclair, and J. H. Warner, Nano Lett. **16**, 1210–1217 (2016).
[36]A. Londoño-Calderon, D. J. Williams, M. M. Schneider, B. H. Savitzky, C. Ophus, S. Ma, H. Zhu, and M. T. Pettes, Nanoscale **13**, 9606–9614 (2021).